Published in final edited form as:

J Phys Chem C Nanomater Interfaces. 2016 October 27; 120(42): 24070–24079. doi:10.1021/acs.jpcc.6b06713.

Versailles Project on Advanced Materials and Standards Interlaboratory Study on Measuring the Thickness and Chemistry of Nanoparticle Coatings Using XPS and LEIS

Natalie A. Belsey[1], **David J. H. Cant**[1], **Caterina Minelli**[1], **Joyce R. Araujo**[2], **Bernd Bock**[3], **Philipp Brüner**[4], **David G. Castner**[5], **Giacomo Ceccone**[6], **Jonathan D. P. Counsell**[7], **Paul M. Dietrich**[8], **Mark H. Engelhard**[9], **Sarah Fearn**[10], **Carlos E. Galhardo**[2], **Henryk Kalbe**[7], **Jeong Won Kim**[11], **Luis Lartundo-Rojas**[12], **Henry S. Luftman**[13], **Tim S. Nunney**[14], **Johannes Pseiner**[15], **Emily F. Smith**[16], **Valentina Spampinato**[5,a], **Jacobus M. Sturm**[17], **Andrew G. Thomas**[18], **Jon P.W. Treacy**[14], **Lothar Veith**[3], **Michael Wagstaffe**[18], **Hai Wang**[19], **Meiling Wang**[19], **Yung-Chen Wang**[4], **Wolfgang Werner**[15], **Li Yang**[20], and **Alexander G. Shard**[1,*]

[1]National Physical Laboratory, Teddington, Middlesex, TW11 0LW, UK [2]Instituto Nacional de Metrologia, Qualidade e Tecnologia (INMETRO), Divisão de Metrologia de Materiais (Dimat) Avenida Nossa Senhora das Graças, 50 Duque de Caxias, RJ 25250-020, Brazil [3]Tascon GmbH, Mendelstr. 17, D-48149 Münster, Germany [4]ION-TOF GmbH, Heisenbergstr. 15, 48149 Münster, Germany [5]National ESCA and Surface Analysis Center for Biomedical Problems, Departments of Bioengineering and Chemical Engineering, University of Washington, Seattle, WA 98195-1653, USA [6]European Commission Joint Research Centre, Institute for Health and Consumer Protection, Nanobiosciences Unit, Via E. Fermi 2749, 21027 Ispra, Italy [7]Kratos Analytical Ltd., Wharfside, Trafford Wharf Road, Manchester M17 1GP, UK [8]BAM Federal Institute for Materials Research and Testing (BAM 6.1), Unter den Eichen 44-46, D-12203 Berlin, Germany [9]Pacific Northwest National Laboratory, EMSL, Richland, WA 99352, USA [10]Department of Materials, Imperial College London, South Kensington Campus, London SW7 2AZ, UK [11]Korea Research Institute of Standards and Science, 267 Gajeong-ro, Daejeon 34113, Korea [12]Instituto Politécnico Nacional, Centro de Nanociencias y Micro y Nanotecnologías, UPALM, Zacatenco, México D.F. CP. 07738, México [13]Surface Analysis Facility, Lehigh University, 7 Asa Drive, Bethlehem, PA 18015. USA [14]Thermo Fisher Scientific, Unit 24, The Birches Industrial Estate, Imberhorne Lane, East Grinstead, West Sussex, RH19 1UB, UK [15]Institut fuer Angewandte Physik, TU Vienna, Wiedner Hauptstr 8-10, A 1040 Vienna, Austria [16]Nanoscale and Microscale Research Centre, School of Chemistry, University of Nottingham, University Park, Nottingham NG7 2RD, UK [17]Industrial Focus Group XUV Optics, MESA+ Institute for Nanotechnology, University of Twente, P.O. Box 217, 7500 AE Enschede, the Netherlands [18]School of Materials and Photon Science Institute, University of Manchester, Manchester, M13 9PL, UK [19]National Institute of Metrology,

[*] alex.shard@npl.co.uk, AUTHOR TELEPHONE NUMBER: +44 20 8943 6193.
[a]current address: IMCACSA, IMEC, Kapeldreef 75, 3001 Leuven, Belgium.

SUPPORTING INFORMATION: Protocol for sample preparation circulated to study participants; calculation of nanoparticle shell thickness by XPS using the T_{NP} equation; supplementary figures include an example XPS C1s narrow scan and photographs of type B samples deposited by participants.

Beijing 100029, P. R. China [20]Department of Chemistry, Xi'an-Jiaotong Liverpool University, Suzhou, China.

Abstract

We report the results of a VAMAS (Versailles Project on Advanced Materials and Standards) inter-laboratory study on the measurement of the shell thickness and chemistry of nanoparticle coatings. Peptide-coated gold particles were supplied to laboratories in two forms: a colloidal suspension in pure water and; particles dried onto a silicon wafer. Participants prepared and analyzed these samples using either X-ray photoelectron spectroscopy (XPS) or low energy ion scattering (LEIS). Careful data analysis revealed some significant sources of discrepancy, particularly for XPS. Degradation during transportation, storage or sample preparation resulted in a variability in thickness of 53 %. The calculation method chosen by XPS participants contributed a variability of 67 %. However, variability of 12 % was achieved for the samples deposited using a single method and by choosing photoelectron peaks that were not adversely affected by instrumental transmission effects. The study identified a need for more consistency in instrumental transmission functions and relative sensitivity factors, since this contributed a variability of 33 %. The results from the LEIS participants were more consistent, with variability of less than 10 % in thickness and this is mostly due to a common method of data analysis. The calculation was performed using a model developed for uniform, flat films and some participants employed a correction factor to account for the sample geometry, which appears warranted based upon a simulation of LEIS data from one of the participants and comparison to the XPS results.

Graphical Abstract

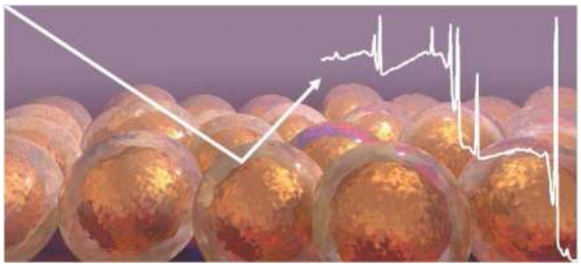

INTRODUCTION

Engineered nanoparticles are of major importance as enabling components for novel technologies, such as drug delivery vehicles,[1,2] medical diagnostics,[3,4] sensors,[5,6] batteries[7,8] and opto-electronic devices.[9-12] Their utility is constrained by the fine tolerances required for size, shape, dispersity, aggregation state and ability to interact appropriately with other functional elements. To establish the causes of variable performance, to ensure batch-to-batch consistency and to assist the scale-up of nanoparticle production, it is important to be able to measure the properties of particles that define performance. Such measurements need to be sufficiently sensitive and precise in order to identify any deviations that affect the product and, for the purpose of assurance, they need to be reproducible. Reproducibility will enable comparability in measurements between manufacturers and

users of nanomaterials and establish confidence in the supply chain, thereby reducing the costs of development and quality procedures.

To modify the aggregation state, external interactions and, in some cases, the functional performance of nanoparticles it is necessary to have control over the surface chemistries. The measurement of surface chemistry has received less attention than particle size, possibly because quantitative measurements are difficult to perform *in-situ* and require the use of specialized instruments. One of the most appropriate methods, which provides quantitative information on surface elemental composition, some chemical state information and an information depth consistent with nanoparticle dimensions is X-ray photoelectron spectroscopy (XPS). This method has been employed routinely for many decades to study the surfaces of nanoparticles used in supported heterogeneous catalysis, and is increasingly being used to measure the properties of nanoparticles used for medical and optoelectronic applications.[13-17] Recent reports have indicated that ion scattering methods, such as low and medium energy ion scattering (LEIS and MEIS) may be employed as a sensitive method for measuring the coating thickness of nanoparticles.[18,19] There are a number of challenges that analysts face when they employ ultra-high vacuum techniques to characterize nanoparticles.[20] The purpose of this study was to determine the most significant analytical challenges, to assess their significance and to identify actions to ameliorate the most important of these.

SAMPLES

Citrate-stabilized gold NPs of diameter 59 nm were purchased from BBI Solutions (Cardiff, UK). Citrate coated NPs were imaged by Scanning Electron Microscopy (SEM) using a Zeiss (Oberkochen, Germany) Supra Microscope (In lens, 30 μm aperture, 10 kV) to assess the assumption of NP sphericity. The diameter was confirmed by dynamic light scattering and the polydispersity index was determined to be 0.13 by measurements in triplicate. The buffer 3-[4-(2-Hydroxyethyl)-1-piperazinyl]propanesulfonic acid (EPPS) was obtained from Sigma Aldrich (St Louis, MO, USA). The CAG4 peptide (CGGGNPSSLFRYLPSD)[21] was purchased from GenScript (Piscataway, NJ, USA). All NP suspensions were prepared and stored in Eppendorf (Hamburg, Germany) LoBind tubes as a precaution against peptide loss by adsorption.

A suspension of peptide-coated NPs was prepared by the addition of citrate-stabilized gold NPs to an equal volume of peptide solution (0.034 g L^{-1}, i.e. 20 μM, CAG4 peptide in 10 mM EPPS buffer). Incubation was performed at room temperature for 1 hour, with gentle shaking. The suspension was then subjected to centrifugation washes to remove traces of buffer salts and unbound peptide. Three centrifugation cycles (1 hour, 180 RCF, Eppendorf 5430 centrifuge) were performed during which most of the supernatant was removed, and the pellet from each 2 mL tube was re-suspended in ultrapure water. After the final spin, the supernatant was removed and the pellet (~ 50 μL) was collected and recombined to one large batch (estimated final concentration ~5 $\times 10^{11}$ NPs per mL). The batch was then divided in two: one half was used to prepare 35 ready-deposited samples for distribution, the other half was divided into 35 smaller Eppendorf tubes for distribution as a concentrated suspension. Silicon wafer with 100 surface orientation (University Wafer, Boston, MA, USA) was cut

into 70 squares of 1 × 1 cm^2. The wafer was cleaned by soaking in isopropyl alcohol and dried under a stream of nitrogen. A 6.07 mm bore Viton rubber O-ring (RS Components, Corby, UK) was placed centrally on to each of 35 substrates to reduce coffee-ring effects caused by differential evaporation rates. Aliquots of the concentrated peptide-coated nanoparticle suspension (3 μL per substrate) were applied to the center of each O-ring (without making contact with it) and allowed to dry under vacuum in a desiccator before the addition of a further aliquot on top of each spot (Figure 1B). This was repeated until the entire aliquot had been utilized (170 μL per sample), *i.e.* more than 50 aliquots of suspension, with an 8 hour preparation time.

Silicon wafer coated with 100 nm gold (Platypus Technologies, Madison, WI, USA) was cleaned with ethanol and water and dried under a stream of nitrogen both before and after 20 minutes of ultraviolet ozone cleaning (T10X10 ozone cleaner, UVOCS, Montgomeryville, PA, USA). Peptide functionalization of flat gold was performed by soaking the cleaned gold surface in the peptide solution. The substrates were incubated for one hour at room temperature before the surfaces were rinsed with ultrapure water and gently dried under a stream of nitrogen.

The samples deposited on to silicon substrates were stored and transported in Fluoroware wafer shipping containers (Entegris, Billerica, MA, USA). These are referred to as sample type ‘A’. The containers incorporated a flexible plastic ‘spider’ to prevent sample damage by rattling during shipping. As a precaution against oxidation or other forms of degradation, the samples were transported within sealed bags containing an argon atmosphere, and upon receipt, participants were instructed to place the whole unopened bag directly into a refrigerator (2-5 °C) for storage. The samples were transported with temperature indicators to alert the recipient if the nanoparticle solutions were subjected to freezing temperatures during transit which could compromise their integrity. Participants were instructed to allow at least one hour for the samples to return to room temperature before opening the Fluoroware container, and in addition, that samples should only be handled at their edge using cleaned metal tweezers held using powder-less polyethylene gloves.

All participants were sent the protocol for sample preparation and analysis (Supplementary Information S1). This document provided guidance for sample handling in addition to a suggested method for depositing the NPs from suspension which was identical to the procedure described above for sample type ‘A’. Participants prepared their own samples from the suspension provided to them, using the method provided as guidance, these are referred to as sample type ‘B’. Both sample types ‘A’ and ‘B’ were analyzed using either XPS or LEIS by each participant.

ANALYSIS

Due to the variety of instruments used in the study, no single set of instrumental operating conditions could be specified for either XPS or LEIS. Therefore, participants were instructed to use instrument settings which would give the most reliable performance. Participants were requested to perform analysis in triplicate on three non-overlapping regions of each sample, with minimal exposure to elevated temperatures. The data was reported as equivalent atomic

%, assuming homogeneous distribution of the elements using participants' standard procedures and wide-scan spectra were also returned to NPL for detailed analysis.

Participants were invited to use their own in-house procedures to calculate the thickness of the peptide coating, and after completing their analysis to return the samples to NPL. However, not all participants were able or willing to attempt this calculation.

PARTICIPANTS

Samples were distributed to 25 different laboratories for analysis; with some receiving multiple sample packs for analysis using different instruments. Data was returned by 20 participants, 16 participants used XPS and 5 participants used LEIS. Participants are designated with letters; A-P used XPS; Q-U used LEIS; one laboratory returned both LEIS and XPS data, and has been designated separate letters for each instrument. Instrumentation and sample preparation details for each participant are listed in Table 1. A number of participants attempted a MEIS analysis of these samples, but this technique proved unsuitable for these particular samples and therefore it is not included in this work.

RESULTS AND DISCUSSION

XPS results

The participants provided both wide-scan and narrow-scan XPS spectra and the results of their analyses: the areas of the Au 4f doublet, the C 1s, N 1s and O 1s peaks after background subtraction and an estimate of the composition of the sample using their standard procedures and assuming homogeneous elemental distribution in the sample. Some participants noted the presence of other elements in some areas of the sample: typically excess sulfur, as well as silicon and sodium. This was quite rare on sample type 'A', but more common in sample type 'B' in which the presence of silicon was consistent with incomplete coverage of the silicon wafer substrate. Data in which these elements contributed more than 2 at.% to the estimated composition were excluded from further analysis and, for lower concentrations of these elements, the homogeneous compositions renormalized and expressed as atomic fractions after excluding all elements except Au, C, O and N.

In Figure 1 we plot the thickness of sample type 'A' reported by the participants, T_A, against the fraction of gold reported assuming homogeneity, [Au], as filled symbols (■,◆).The reported compositions, [Au], range from ~0.1 to ~0.3 and the reported thicknesses, T_A, span an order of magnitude from ~0.5 nm to ~5 nm. There appears to be little correlation between T_A and [Au]. This is rather surprising because the essential calculation should result in an anti-correlation: as the shell thickness gets smaller the fraction of gold detected in XPS should get larger, an indicative line on the graph describes the expected relationship.

Participants indicated by the diamond symbol (◆) used a variety of methods to calculate T_A: participant F used an iterative approach; G and O calculated the thickness assuming a flat surface; participant I calculated the thickness assuming a flat surface and then halved the result. This latter approach is valid in the case of large particles of 100 nm diameter or greater with shells of the order of atomic thickness.[22] The line shown on the graph results

from an implementation of the T_{NP} formula,[23] which was also the method employed by participants H, J, K, L, M, N and P indicated by square filled symbols (■). The T_{NP} equation is provided in the Supplementary Information. The difference between the line and square filled symbols is rather large in some cases and the cause of this difference is largely due to the reference intensities used by participants. These reference intensities are required to normalize the peak areas obtained from the spectrum to obtain parameter A, as described in Equation (1), where, I_{Au} is the measured gold core intensity, and I_k is the measured intensity of one of the elements, k, in the shell. The superscript '∞' indicates the intensities are measured or estimated from flat samples of pure gold or pure shell material respectively and are termed the reference intensities.

$$A_k = \frac{I_k I_{Au}^{\infty}}{I_{Au} I_k^{\infty}} \quad (1)$$

In practical applications, it is convenient to convert the equation for A into a form suitable for the direct input of fractional compositions calculated using the assumption of homogeneity.[14] Equation (4) provides this conversion, in which S_i is the relative sensitivity factor for photoelectrons from element i, X_k is the fractional composition of element k in the shell material (*i.e.* excluding elements in the core), square brackets, [i], represent the XPS fractional compositions calculated using the assumption of homogeneity (*i.e.* including elements in the core), and f represents a factor that takes into account the differences in atomic densities and electron attenuation lengths between the two materials and also any bias introduced by electron energy loss processes and background subtraction methods. The value of f may be estimated, but is best established by experiment on suitable pure and flat reference materials.

$$A_k = \frac{I_k I_{Au}^{\infty}}{I_{Au} I_k^{\infty}} = f \frac{I_k S_{Au}}{I_{Au} S_k X_k} = f \frac{[\mathrm{k}]}{[Au]\, X_k} \approx f \frac{1 - [Au]}{[Au]} \quad (2)$$

The final, approximate, form in equation (2) assumes that all elements except gold are in the particle shell and that suitable 'average' values for attenuation lengths can be found. Otherwise, all elements can be separately treated using the T_{NP} equation and the X_k iteratively adjusted, under the constraint $\sum X_k = 1$, to obtain a unique solution where all values of $L_{k,a}$ T_{NP} (A_k) are identical. In this manner both the elemental composition and the thickness of the shell may be determined.

In Figure 1, the solid line is calculated using the approximate form of equation (2) with f = 0.56,[14,24] which was established using flat, pure reference materials on a spectrometer with a calibrated transmission function[25] using average matrix relative sensitivity factors (AMRSFs)[26] and attenuation lengths taken from Seah's equations.[27] The open symbols (□) represent a treatment of the participants' reported elemental compositions using the iterative method described above and the thickness result from this method is in good agreement with the approximate form of equation (2). We note that participant P employed SESSA[28] software to calculate reference intensities (SESSA uses an accurate description of electron

emission and transport) and obtained a result insignificantly different from the line. Participant L used Mg Kα radiation, as opposed to Al Kα used by other participants, therefore the electron energies and attenuation lengths are smaller and their data point falls upon a different line to the one shown, which passes through the open symbol marked (L).

Note that, even after the application of a common method to translate the XPS data into a thickness, there is significant scatter in the calculated thickness, ranging from 1.78 nm (participant C) to 4.62 nm (participant I). This relates to the reported fraction of gold and may be caused either by variability amongst the samples of type 'A', the XPS instrumentation or data interpretation.

Comparison of the composition of the shell calculated using the iterative method described above demonstrated good agreement between participants. The fraction of nitrogen in the shell, X_N, had a mean value of 13.8 at.% with a relative standard deviation (RSD) between participants of 9 % compared to an average RSD of 7 % from repeat analyses of the same sample by participants. This concordance is a result of the good agreement in the relative sensitivity factor for N 1s compared to C 1s, the mean value of S_{N1s}:S_{C1s} was 1.69 with 4 % scatter. There was poorer consensus on the relative sensitivity factor for Au 4f with a mean value of 21.3 for S_{Au4f}:S_{C1s} with 12 % scatter even after excluding the value of S_{Au4f}:S_{C1s} = 9.58 for participant C, which appears to be an erroneous use of the sensitivity factor for the Au $4f_{7/2}$ peak rather than that for the combined Au $4f_{7/2}$ and Au $4f_{5/2}$ doublet. After correcting this error, the calculated value of shell thickness for participant C changed from 1.78 nm to 2.93 nm. However, an attempt to adjust other data using a common set of sensitivity factors did not significantly reduce the scatter in calculated thicknesses. The RSD in calculated thickness between participants changed from 22 % to 21 %. Comparing this to the typical scatter (RSD < 4 %) from repeat analyses of the same sample by most participants, it is clear that disparate sensitivity factors are not the most important cause of discrepancy.

Figure 2 displays wide-scan XPS spectra supplied by participants. In panel 2a data from four participants: B, C, I and H are overlaid and the intensity normalized so that the region in the vicinity of the N 1s peak at binding energy (BE) ~400 eV, kinetic energy (KE) ~1086 eV, is closely matched. Here, it is clear that the intensities and backgrounds from the O 1s to the C 1s peaks are similar, but there is strong divergence outside this region and, for a number of participants, a somewhat different intensity for the Au 4f peaks. If this effect was due to a different shell thickness, the same effects (changed peak and background intensity) evident for the Au 4f peak should occur for all other gold peaks, including the Au 4d peaks. An example is provided by data from participant G in panel 2b. This participant experienced problems with sample damage during analysis, resulting in a loss of the organic shell. As the shell thickness changes, the peak and background in the region of the Au 4f peaks change, but the effect is even stronger for the Au 4d peaks. No such variation in the Au 4d region is evident in other participants' data, implying that sample to sample variation is not the cause of variable Au 4f intensity. The remaining explanation is that there are significant differences in the transmission functions as discussed by Smith and Seah[29] or in the correction procedures used by participants. One may expect that the sensitivity factors used by participants should compensate for such effects, but in many cases it is clear that they

actually exacerbate the discrepancies. This highlights the need for XPS users to ensure that transmission functions and sensitivity factors are obtained from a consistent source or, alternatively, to regularly update their instrumental sensitivity factors using appropriate standard materials so that changes in instrument transmission can be accounted for.

Since post-hoc adjustment of transmission function correction procedures were not possible, analysis of the wide-scan spectra was performed at NPL using the intensities of the Au 4d peaks, rather than the Au 4f peaks, along with the C 1s, N 1s and O 1s. In this region of the spectra there appear to be only minor variations in relative instrumental transmission between participants. For practical reasons background subtraction for the Au 4d peaks was performed using Shirley backgrounds and linear backgrounds used for the other peaks and AMRSFs used to calculate equivalent homogeneous compositions. Equation (2) was applied to these compositions to calculate shell thickness and shell composition and the factor f = 0.39 for the Au 4d peaks found by matching the calculated thickness from NPL preliminary samples to that found using the Au 4f peaks with f = 0.56 and a Tougaard background. Note that the Shirley background typically underestimates the area of an XPS peak compared to the Tougaard background and so this reduction in the value of f is expected. Following this treatment, far better reproducibility was found, with an RSD between participants of 13 %, which includes some participants, such as G, where sample damage during analysis is evident. Excluding these, the agreement between participants is significantly better than 10 %. The relative accuracy of the mean shell thickness, $T_{A,\,Au4d}$, of 2.82 nm, relies upon the accuracy of attenuation lengths, relative pure material intensities and the T_{NP} formula, and amounts to ~12 %.

An advantage of XPS analysis over many other methods is that the analysis provides quantitative chemical information. In this case, the composition of the shell material may be found using the method described above. In Figure 3, the results of the analysis performed at NPL using the Au 4d peaks to determine shell thickness are presented and good agreement is found between all participants.

In panel 3a the fraction of nitrogen in the shell, X_N, calculated from participants' data is presented and in panel 3b, the fraction of oxygen in the shell, X_O. The solid lines represent the average result and the dashed line the fraction calculated from the peptide composition assuming a homogeneous distribution of the elements in the shell. The RSD between participants is ~9 % in both cases. The carbon content of the shell, X_C, was 68 ± 3 %, larger than the expected 61 % based upon the peptide composition and this is probably due to some hydrocarbon contamination, which is not uncommon and has been noted previously on nanoparticle samples of this type.[15] It is also worth noting that the line-shape of the C 1s spectra for sample type 'A' were consistent with the peptide composition, showing a clearly resolved peak at the position expected for the amide group. An example is provided in the Supplementary Information, Figure S6.

LEIS results

Five participants, Q to U, employed LEIS to measure the shell thickness on sample type 'A'. Of these all except participant U provided an analysis of the data and a value for the thickness of the shell. Three of these used a method described by Brongersma *et al.* for flat

gold samples coated with thiol monolayers[30] and used by Rafati *et al.* for gold particles coated with a thiol monolayer.[18] The data provided by participant U was analyzed at NPL using the same method and the principle is outlined in Figure 4.

Helium ions are scattered from the sample and collected at a fixed scattering angle. The energy loss in the scattering process contains information on the mass of the atom that the helium ion scattered from and the depth at which the scattering event occurred. Two spectra are shown on different ordinate scales: clean gold is plotted against the right hand ordinate and sample type 'A' on the left hand ordinate. The prominent peak in the clean gold spectrum is due to scattering from surface gold atoms and the weak tail at lower energies due to scattering from subsurface gold atoms and loss of kinetic energy as the ion travels in and out of the material. The weak intensity is caused by neutralization of the helium ions, scattered neutrals are not detected as LEIS instruments are generally only configured to detect ions. For sample type 'A' there is no surface peak for gold which demonstrates that there are no defects in the shell. Only subsurface scattering is present and the high energy onset of this scattering provides a measure of the distance the helium ions have traversed to reach the core of the particle. Following the method of Brongersma, this data is fitted with an error function, in this case convoluted with a linear function to account for the general loss in intensity toward lower kinetic energy. The energy difference between the inflexion point of the fit and the surface gold scattering maximum is assumed to be proportional to the thickness of the coating. For planar alkanethiol monolayers on gold, Brongersma[30] found 8 eV/carbon atom for 1.5 keV $^4He^+$. Rafati *et al*,[18] converted this into 90 eV/nm in organic materials for 3 keV $^4He^+$. This value was used by most participants and the energy difference of 347 eV in Figure 4 translates to 3.86 nm equivalent planar thickness. Participant R followed this method and found 3.43 ± 0.06 nm. Participants Q and T used the same method, but applied a factor of 0.74 to account for the spherical topography of the sample. This factor resulted from detailed calculations, but is not yet reported in the literature. Participant S compared their data to simulations that take into account the particle geometry and scattering geometry, and reported a thickness of 3.0 nm.

Comparison of thickness measurements

In Figure 5, the thicknesses for the peptide shell from sample type 'A' for all participants are compared.

Panel 5a displays the XPS results calculated from the Au 4d peaks, $T_{A,\,Au4d}$, and shows that good comparability can be obtained, although participants G and J have significantly lower thicknesses as do A and O to a lesser extent. Participant G had issues with sample degradation during analysis, as indicated in panel 2b, possibly caused by the use of a micro-focused X-ray beam. Participants A and O also used micro-focused beams, but participant J did not and, since participants C, D and K also used focused X-ray sources, it is not clear whether this is the cause of sample degradation. The result for participant H indicates a thicker shell (3.5 nm) than other participants and, since the composition of the shell is not inconsistent with other participants, this may result from a difference in the sample itself. Panel 5b displays the thickness of sample type 'A' determined by LEIS using the Brongersma method for flat surfaces, $T_{A,\,flat}$, and panel 5c the same results after application

of the 0.74 topography factor, $T_{A,\,topo}$. The value for participant S was calculated using a different method, as described above. The mean thicknesses in the two cases are, 3.63 nm and 2.75 nm, the second being rather close to the mean XPS thickness of 2.82 nm. The XPS value has a relative uncertainty of ~0.35 nm and the LEIS thickness uncertainty is somewhat unclear at this stage. However, this comparison indicates that a topographic correction is required for LEIS data from surfaces which are not flat.

Sample preparation by participants

The participants, apart from S and P, prepared their own samples from a suspension of nanoparticles of the same batch that was used to prepare sample type 'A'. The procedure provided to them in the protocol (Supplementary Information, S1) was essentially identical to the one used to prepare sample type 'A'. However, it is a lengthy procedure and, since some participants did not have access to a vacuum desiccator, the procedure took many days in some cases. The prepared samples were returned to NPL for inspection and it is clear that, in some cases, insufficient coverage of the silicon wafer substrate was obtained (see Supplementary Information, Figure S7). For participants using XPS this was apparent also in the presence of silicon and oxygen detected in the spectra. In these cases, carbonaceous contamination on the substrate would also contribute to the C 1s intensity and would result in an apparently thicker organic shell. In Figure 6, the majority of results from participants are presented.

Panel 6a displays the calculated thickness for sample type 'B', T_B, plotted against the calculated thickness, using the same method, for sample type 'A', T_A. The variation in results from repeat experiments is indicated by the error bars representing one standard deviation. For XPS participants, shown as open circles (○), the calculation is based upon the reported fraction of gold, using the T_{NP} formula and the approximate form of equation (4). Results from participants C, I and M are excluded from the figure due to the contributions from elements such as silicon and sodium exceeding 4 at. %. Notably, these three participants did not have access to a vacuum desiccator and reported the longest preparation times. For LEIS participants (■), the values were calculated by the method of Brongersma with the application of a 0.74 geometry factor. If sample type 'A' and 'B' were identical, the results should fall on the line $T_B = T_A$ which is shown on the graph. It is clear that, in general, these samples are not identical and sample type 'B' has an apparently thicker shell than sample type 'A'. This is true also for LEIS participants whose data should not be affected by substrate contributions. For XPS participants, even when no substrate contribution was evident, the increase in apparent shell thickness was associated with a larger C 1s signal, without a concomitant increase in N 1s intensity, as demonstrated in panel 6b where the apparent fraction of nitrogen in the shell is seen to decrease as the thickness increases. These results are consistent with sample contamination, possibly coupled with degradation, which may have occurred during the preparation procedure, or during transit and storage. Such contamination is of major importance when the shell or core material contains carbon, but may be less important if they do not. However, for detailed work, it is important to identify such contamination on particles as it will influence the intensity of signals from the core and the shell due to electron attenuation effects. Perhaps of greater concern is the observation that, even in the case that T_B is only slightly larger than T_A, there

is a significant drop in the nitrogen composition, X_N, of the shell material. This indicates that the samples have degraded either during transport, storage or preparation for analysis. Such effects are not evident in sample type 'A'. This indicates that, for materials with organic shells at least, preparation for analysis should be performed as soon as possible after production and the samples transported and stored in dry conditions.

Discussion

This study has enabled a clear assessment of the sources of uncertainty in measuring the composition and shell thickness of core-shell nanoparticles using XPS and LEIS. Sample preparation is a clear cause for concern. These were particularly challenging samples to prepare for analysis, particularly by XPS, as can be seen from the scatter in Figure 6. The LEIS results are rather consistent because the method assesses only the thickness of material over the gold core and therefore contamination underneath the first layer of particles does not influence the measurement. For XPS, and in the case of organic shells, the issue of sample preparation is more acute since it is difficult to distinguish the contribution of organic contamination on the substrate or between the particles from the shell material. Comparing the ratio of thicknesses determined from sample type 'B' to sample type 'A' and using a consistent measurement of thickness we find that the LEIS results provide a mean thickness for sample type 'B' which is 4/3 larger than for sample type 'A', with a very low scatter (RSD) of 4.9 % for $T_B : T_A$. The XPS results are not inconsistent with these findings, but much more highly scattered with an RSD of 53 % for $T_B : T_A$. This is one of the major sources of discrepancy between participants, but it is not the major source of variability for XPS participants.

For participants using XPS, we identified two other sources of poor comparability: the conversion of XPS spectra into equivalent homogeneous compositions and the conversion of XPS intensities into shell thickness. In this work, these are intimately linked, but they need not be. Comparison of the reported gold composition [Au] from the Au 4f peak intensities to that calculated from the Au 4d peaks in the wide-scan spectra for sample type 'A' demonstrates high variability. The RSD of the ratio of these values is 33 %. This variability can largely be ascribed to transmission function correction procedures and choice of relative sensitivity factors and would contribute 21 % variability to the value of T_A. Of more importance is the choice of methods to convert XPS data into shell thickness. Here, we can compare the reported values from participants to that calculated from the reported values of [Au] using the T_{NP} method, equation 4 and attenuation lengths from Seah.[27] The essence of this comparison is demonstrated in Figure 1 using the ratios of the reported values of T_A (filled symbols) to the NPL calculated values (open symbols), the scatter in these ratios is large with an RSD of 67 % and is the most significant source of discrepancy. The participants using LEIS were in closer agreement than those using XPS and this is, in part, due to the use of a common analysis method and reference data.

CONCLUSIONS

This inter-laboratory study has shown that it is possible to measure the shell thickness of core-shell nanoparticles and obtain consistent results. Following careful analysis of samples

prepared by a common method and using a common data analysis approach agreement on shell thickness and composition using XPS was approximately 10 %. A similar level of agreement between participants using LEIS to measure shell thickness was also obtained, and was also in reasonable agreement with the mean XPS thickness. These results demonstrate that, with consistent procedures, both methods are capable of providing reliable and comparable measurements of nanoparticle coatings, the detail and precision that can be obtained from these methods is difficult to obtain in other ways. However, several important challenges for this type of measurement were identified in this study:

Sample type 'B' prepared by participants from colloidal suspensions produced highly variable results. This may partly be caused by degradation of the particles during transportation and storage, but is also due to the preparation methods used by participants. There was far less variability in the results from sample type 'A' prepared at NPL and this suggests a need for appropriate documentation and controls describing preparation methods and sample history. The XPS results suggest that samples of this type should be prepared for analysis as soon as possible and transported and stored in a dry condition.

The calculation of shell thickness by participants using XPS was a major source of poor comparability. The primary cause of this appears to be related to the estimation or measurement of reference intensities, a secondary cause being the use of different methods to account for the geometry of the sample. This finding relates not only to the measurement of nanoparticles, but is important for any calculation of thickness by XPS. Clearly, there are inadequate, or contradictory, resources for XPS analysts when such calculations are performed. This may be resolved by establishing useful databases and standardized methods.

A further issue, of more general importance to reliable and trustworthy XPS analysis, was highlighted in this study. The high (33 %) variability in the reported gold compositions of the sample is a cause for concern. This was shown not to be due to variability in the samples themselves but due to an inconsistent application of transmission function correction and relative sensitivity factor values. Repeat analyses by participants indicates that repeatability in the same laboratory is very good, a variability of a few percent in most cases, so this poor reproducibility between laboratories is surprising. We show that careful choice of peaks in the XPS spectrum can ameliorate this problem, but there is a more general need for a standardized approach to enable comparable measurements in different laboratories.

Supplementary Material

Refer to Web version on PubMed Central for supplementary material.

ACKNOWLEDGMENT

We thank Steve A. Smith from NPL for preparing the silicon substrates for the samples. This work forms part of the Innovation Research & Development Programme of the National Measurement System of the UK Department of Business, Innovation and Skills and with funding from the HLT04 BioSurf and 14IND12 Innanopart project by the European Union through the European Metrology Research Programme (EMRP) and European Metrology Programme for Innovation and Research (EMPIR). EMPIR and EMRP are jointly funded by the EMPIR participating countries within EURAMET and the European Union.

Y.-C.W. and D.G.C. gratefully acknowledge the support from United States National Institutes of Health grant EB-002027. Y.-C.W. was also supported by the United States National Science Foundation Graduate Research Fellowship Program under Grant No. DGE-1256082. JWK acknowledges the support from Nano Material Technology Development Program (2014M3A7B6020163) of MSIP/NRF.

REFERENCES

1. Cho K, Wang X, Nie S, Shin DM. Therapeutic Nanoparticles for Drug Delivery in Cancer. Clinical Cancer Res. 2008; 14:1310–1316. [PubMed: 18316549]
2. Soppimath KS, Aminabhavi TM, Kulkarni AR, Rudzinski WE. Biodegradable Polymeric Nanoparticles as Drug Delivery Devices. J. Controlled Release. 2001; 70:1–20.
3. Baptista P, Pereira E, Eaton P, Doria G, Miranda A, Gomes I, Quaresma P, Franco R. Gold Nanoparticles for the Development of Clinical Diagnosis Methods. Anal. Bioanal. Chem. 2008; 391:943–950. [PubMed: 18157524]
4. Liu G, Lin Y-Y, Wang J, Wu H, Wai CM, Lin Y. Disposable Electrochemical Immunosensor Diagnosis Device Based on Nanoparticle Probe and Immunochromatographic Strip. Anal. Chem. 2007; 79:7644–7653. [PubMed: 17877418]
5. Benjaminsen RV, Sun H, Henriksen JR, Christensen NM, Almdal K, Andresen TL. Evaluating Nanoparticle Sensor Design for Intracellular pH Measurements. ACS Nano. 2011; 5:5864–5873. [PubMed: 21707035]
6. Herrmann J, Müller K-H, Reda T, Baxter G, Raguse B. d. De Groot G, Chai R, Roberts M, Wieczorek L. Nanoparticle Films as Sensitive Strain Gauges. Appl. Physics Letters. 2007; 91:183105.
7. Hwang TH, Lee YM, Kong B-S, Seo J-S, Choi JW. Electrospun Core–Shell Fibers for Robust Silicon Nanoparticle-Based Lithium Ion Battery Anodes. Nano Letters. 2012; 12:802–807. [PubMed: 22206272]
8. Wang H, Liang Y, Gong M, Li Y, Chang W, Mefford T, Zhou J, Wang J, Regier T, Wei F. An Ultrafast Nickel–Iron Battery from Strongly Coupled Inorganic Nanoparticle/Nanocarbon Hybrid Materials. Nature Comm. 2012; 3:917.
9. Tuncel D, Demir HV. Conjugated Polymer Nanoparticles. Nanoscale. 2010; 2:484–494. [PubMed: 20644748]
10. Wood V, Panzer MJ, Chen J, Bradley MS, Halpert JE, Bawendi MG, Bulović V. Inkjet-Printed Quantum Dot–Polymer Composites for Full Color AC Driven Displays. Advanced Materials. 2009; 21:2151–2155.
11. Kwak J, Bae WK, Lee D, Park I, Lim J, Park M, Cho H, Woo H, Yoon DY, Char K. Bright and Efficient Full-Color Colloidal Quantum Dot Light-Emitting Diodes Using an Inverted Device Structure. Nano Letters. 2012; 12:2362–2366. [PubMed: 22468609]
12. Kamat PV. Quantum Dot Solar Cells. Semiconductor Nanocrystals as Light Harvesters. J. Phys. Chem. C. 2008; 112:18737–18753.
13. Cant DJ, Syres KL, Lunt PJ, Radtke H, Treacy J, Thomas PJ, Lewis EA, Haigh SJ, O'Brien P, Schulte K. Surface Properties of Nanocrystalline PbS Films Deposited at the Water–Oil Interface: A Study of Atmospheric Aging. Langmuir. 2015; 31:1445–1453. [PubMed: 25557338]
14. Belsey NA, Shard AG, Minelli C. Analysis of Protein Coatings on Gold Nanoparticles by XPS and Liquid-Based Particle Sizing Techniques. Biointerphases. 2015:10.
15. Techane S, Baer DR, Castner DG. Simulation and Modeling of Self-Assembled Monolayers of Carboxylic Acid Thiols on Flat and Nanoparticle Gold Surfaces. Anal. Chem. 2011; 83:6704–6712. [PubMed: 21744862]
16. Techane SD, Gamble LJ, Castner DG. X-Ray Photoelectron Spectroscopy Characterization of Gold Nanoparticles Functionalized with Amine-Terminated Alkanethiols. Biointerphases. 2011; 6:98–104. [PubMed: 21974680]
17. Techane SD, Gamble LJ, Castner DG. Multitechnique Characterization of Self-Assembled Carboxylic Acid-Terminated Alkanethiol Monolayers on Nanoparticle and Flat Gold Surfaces. J. Phys. Chem. C. 2011; 115:9432–9441.

18. Rafati A, ter Veen R, Castner DG. Low-Energy Ion Scattering: Determining Overlayer Thickness for Functionalized Gold Nanoparticles. Surf. Interface Anal. 2013; 45:1737–1741.
19. Sanchez DF, Moiraghi R, Cometto FP, Perez MA, Fichtner PFP, Grande PL. Morphological and Compositional Characteristics of Bimetallic Core@Shell Nanoparticles Revealed by MEIS. Appl. Surf. Sci. 2015; 330:164–171.
20. Baer DR, Amonette JE, Engelhard MH, Gaspar DJ, Karakoti AS, Kuchibhatla S, Nachimuthu P, Nurmi JT, Qiang Y, Sarathy V, Seal S, Sharma A, Tratnyek PG, Wang CM. Characterization Challenges for Nanomaterials. Surf. Interface Anal. 2008; 40:529–537.
21. Naik RR, Stringer SJ, Agarwal G, Jones SE, Stone MO. Biomimetic Synthesis and Patterning of Silver Nanoparticles. Nature Materials. 2002; 1:169–172. [PubMed: 12618805]
22. van Poll ML, Khodabakhsh S, Brewer PJ, Shard AG, Ramstedt M, Huck WTS. Surface Modification of PDMS Via Self-Organization of Vinyl-Terminated Small Molecules. Soft Matter. 2009; 5:2286–2293.
23. Shard AG. A Straightforward Method for Interpreting XPS Data from Core-Shell Nanoparticles. J. Phys. Chem. C. 2012; 116:16806–16813.
24. Ray S, Steven RT, Green FM, Hook F, Taskinen B, Hytonen VP, Shard AG. Neutralized Chimeric Avidin Binding at a Reference Biosensor Surface. Langmuir. 2015; 31:1921–1930. [PubMed: 25650821]
25. Seah MP. A System for the Intensity Calibration of Electron Spectrometers. J. Electron Spectr. Rel. Phenom. 1995; 71:191–204.
26. Seah MP, Gilmore IS, Spencer SJ. Quantitative XPS I. Analysis of X-Ray Photoelectron Intensities from Elemental Data in a Digital Photoelectron Database. J. Electron Spectr. Rel. Phenom. 2001; 120:93–111.
27. Seah MP. Simple Universal Curve for the Energy-Dependent Electron Attenuation Length for All Materials. Surf. Interface Anal. 2012; 44:1353–1359.
28. Smekal W, Werner WS, Powell CJ. Simulation of Electron Spectra for Surface Analysis (SESSA): A Novel Software Tool for Quantitative Auger Electron Spectroscopy and X Ray Photoelectron Spectroscopy. Surf. Interface Anal. 2005; 37:1059–1067.
29. Smith GC, Seah MP. Standard Reference Spectra for X-PS and AES - Their-Derivation, Validation and Use. Surf. Interface Anal. 1990; 16:144–148.
30. Brongersma HH, Grehl T, van Hal PA, Kuijpers NCW, Mathijssen SGJ, Schofield ER, Smith RAP, ter Veen HRJ. High-Sensitivity and High-Resolution Low-Energy Ion Scattering. Vacuum. 2010; 84:1005–1007.

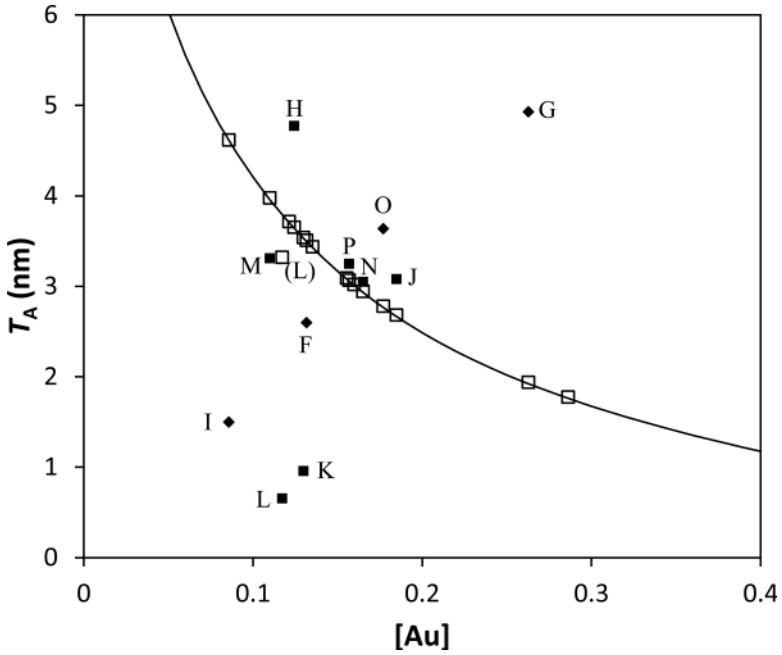

Figure 1.

Comparison of the fraction of gold in the sample [Au] reported by participants to the shell thickness for sample type 'A', T_A, reported by participants (■,◆) and calculated from [Au] using a method described in the text (□). Square symbols (■,□) represent implementations of the T_{NP} method and diamond symbols (◆) represent other methods. The line represents an approximate form of the T_{NP} implementation for Al Kα radiation: participant L employed Mg Kα and therefore the open symbol does not fall on this line.

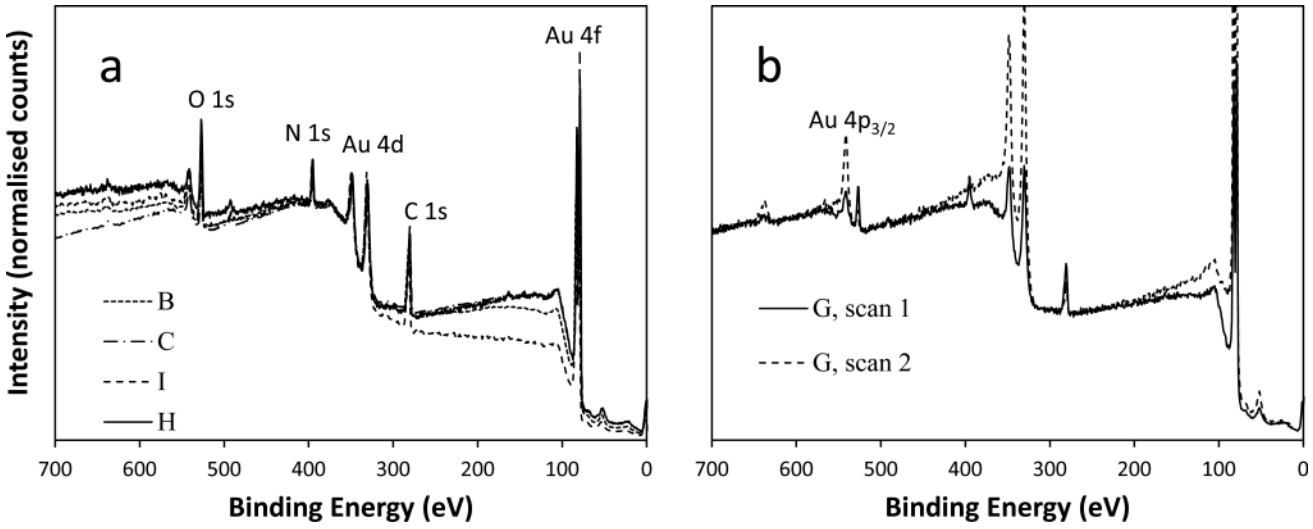

Figure 2.

Wide-scan XPS spectra from sample type ‘A’. (a) Data from participants C, B, I and H demonstrating agreement in the BE region 500 eV to 300 eV and diverging outside this range. (b) Data from participant G showing sample damage in the second scan and the effect of variable shell thickness on the XPS spectrum.

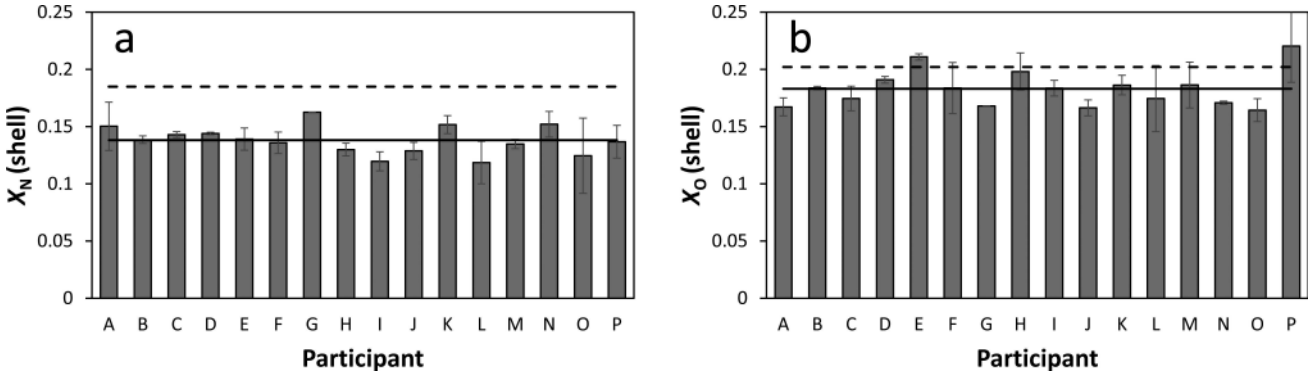

Figure 3.

Elemental composition of the organic shell calculated from XPS participants' wide-scan spectra. The solid line in each panel is the average result, the dashed line is the composition of the pure peptide and error bars represent the standard deviation of repeat measurements. Panel (a) shows the fraction of nitrogen, X_N, and panel (b) shows the fraction of oxygen, X_O. The values are calculated assuming $X_N + X_O + X_C = 1$.

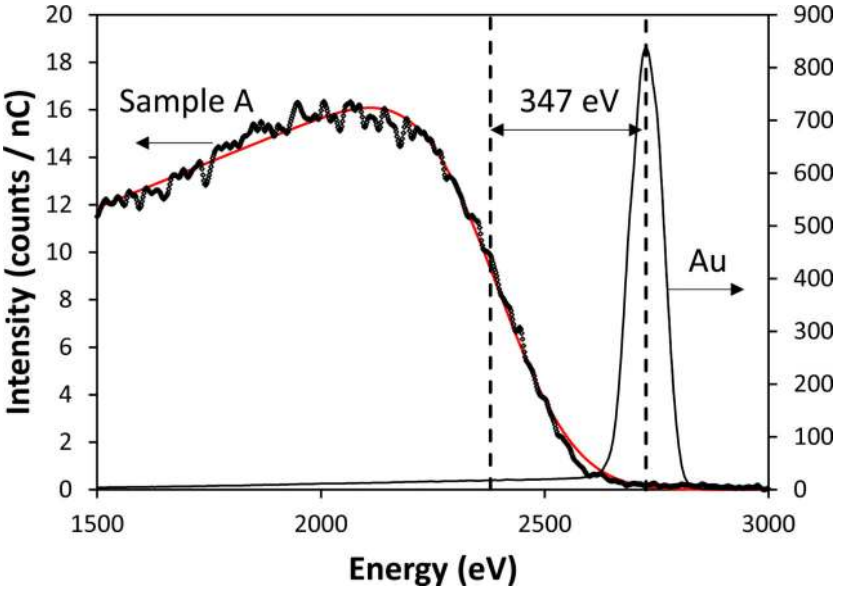

Figure 4.

LEIS data from participant U from sample type ‘A’ (left hand axis) and clean gold (right hand axis). The line shows a fit to the data from sample ‘A’ and the energy difference between the inflexion point of the fit and the maximum of the clean gold surface peak is marked with dashed lines.

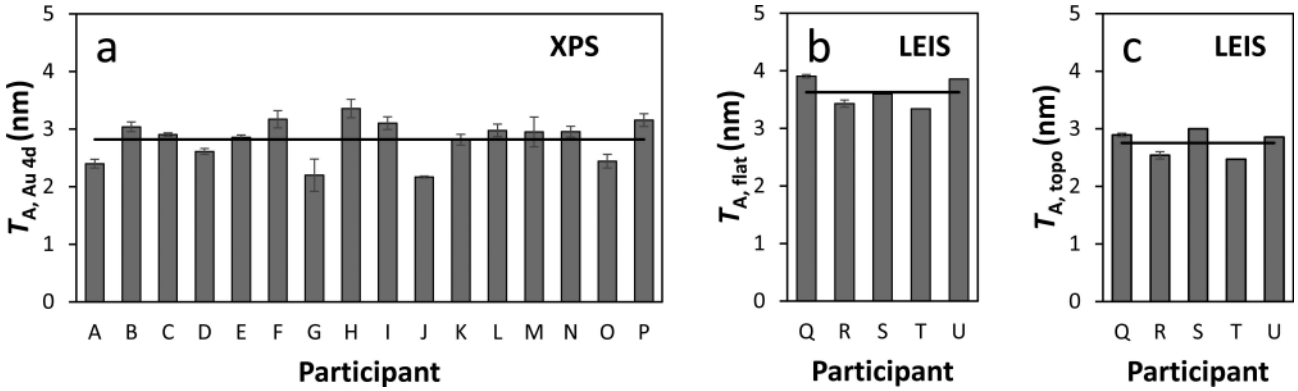

Figure 5.

Comparison of thicknesses for sample type 'A' calculated using participants' data. The average value in each panel is marked with a horizontal line. Panel (a) shows XPS measurements, $T_{A,\ Au\ 4d}$ using wide-scan spectra and Au 4d peak intensities. Panel (b) shows LEIS results using Brongersma's method for flat samples $T_{A,\ flat}$ and panel (c) after the application of a 0.74 correction factor, $T_{A,\ topo}$. The values provided by participant S were calculated by comparison to simulations for a planar surface (b) and a nanoparticle (c).

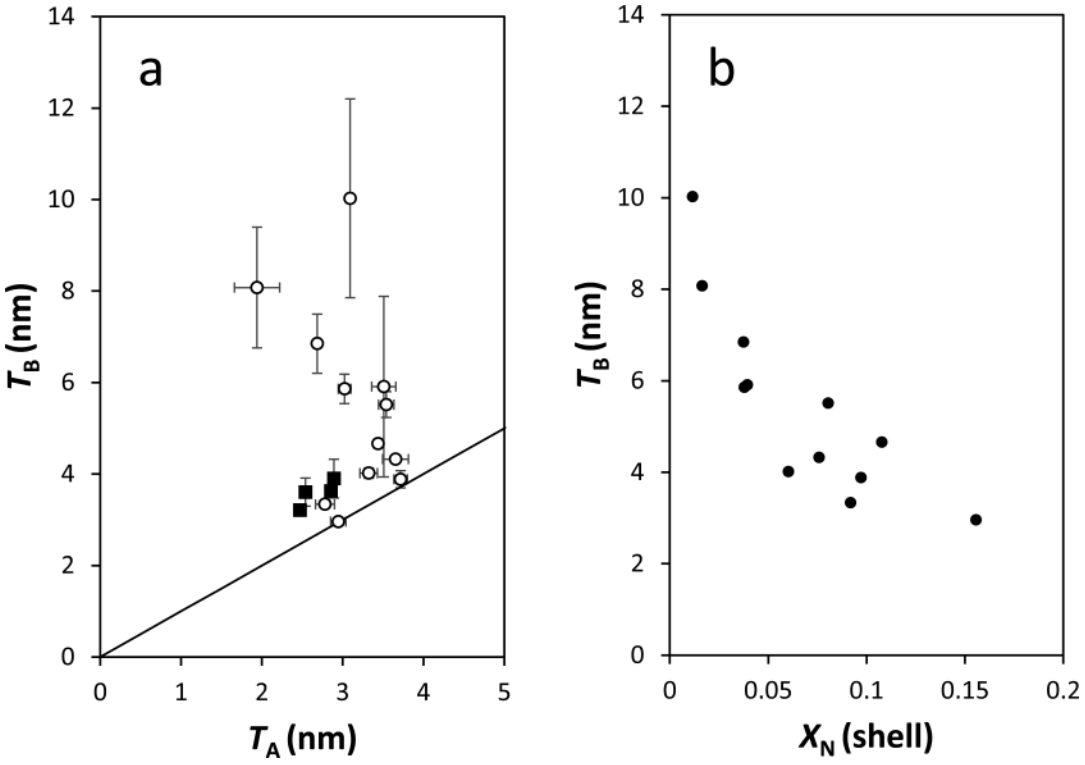

Figure 6.

Results from sample type 'B' prepared by participants. Panel (a) plots XPS (○) and LEIS (■) thicknesses for sample type 'B', T_B, against their result for sample type 'A', T_A. Both values are calculated using the same method and for identical samples should fall on $T_B = T_A$ indicated by the solid line. Panel (b) shows a comparison of the measured shell thickness, T_B, to the fraction of nitrogen in the shell using XPS data, X_N, for sample type 'B'.

Table 1

Participant instrumentation details, sample deposition and thickness calculation methods.

Code	Method	Instrument & beam size on sample	Thickness calculation method	Sample deposition details
A	XPS	Ulvac PHI Quantera SXM, focused X-rays (200 μm)	Not attempted	XPS N_2 entry chamber, 8 hours.
B	XPS	Kratos Axis Ultra (≥1000 μm)	Not attempted	Desiccator, 2 days.
C	XPS	Thermo Fisher K-Alpha+ focused X-rays (400 μm)	Not attempted	No desiccator, 40 hours.
D	XPS	VG ESCALAB 250Xi focused X-rays (400 μm)	Not attempted	Desiccator, 30 hours
E	XPS	Thermo Scientific K-Alpha focused X-rays (400 μm)	Not attempted	No desiccator, 6 hours.
F	XPS	Kratos Axis Ultra (≥1000 μm)	Iterative method	Desiccator, 4.5 days.
G	XPS	Ulvac-Phi PHI5000 VersaProbe II, focused X-rays (100 μm)	Approximated to flat surface	N_2 glove box, 15 hours.
H	XPS	Specs, custom built, Al Kα (1000 μm)	T_{NP} formula	Desiccator, 3 days.
I	XPS	Kratos Axis Ultra (≥1000 μm)	Approximated to flat surface, 0.5 factor	No desiccator, many days.
J	XPS	Kratos Axis Ultra (≥1000 μm)	T_{NP} formula	Laminar flow hood, 2 days.
K	XPS	Thermo Fisher Escalab 250Xi focused X-rays (400 μm)	T_{NP} formula, PET & Au film reference	Desiccator, 20 hours.
L	XPS	Omicron Escaplus P (≥1000 μm)	T_{NP} formula, inorganic carbon reference	Glove box chamber, 2 hours.
M	XPS	Kratos Axis Ultra DLD (≥1000 μm)	T_{NP} formula	Desiccator, 40 hours
N	XPS	Kratos Axis Ultra (≥1000 μm)	T_{NP} formula	Desiccator, 8 hours
O	XPS	ULVAC PHI, PHI Quantera SXM, focused X-rays (100-200 μm)	Approximated to flat surface	Air then vacuum pump station, 14 hours, not all solution deposited.
P	XPS	SPECS GmbH, custom built (400 μm)	T_{NP} formula, SESSA estimation of reference intensities	No details provided
Q	LEIS	IONTOF Qtac 100, He beam, 3 keV 3.9 nA No plasma or ion sputter clean	Brongersma, 0.74 geometry factor	No desiccator, deposited using a wire loop, 5hrs.
R	LEIS	IONTOF Qtac 100, He beam, 3 keV Plasma pre-clean: flat Au only	Brongersma, no geometry factor	No desiccator, 11 days.
S	LEIS	IONTOF Qtac 100, He beam, 3 keV 3.4 nA. Measured before & after cleaning (data used only from untreated samples).	Compared spectra to simulations	Not performed, only pre-deposited sample analyzed.
T	LEIS	IONTOF Qtac 100, He beam, 3 keV 5 nA Plasma and ion sputter clean: only for flat Au reference.	Brongersma, 0.74 geometry factor	Desiccator, 8 hours.
U	LEIS	IONTOF Qtac 100, He beam, 3 keV 15 nA No initial plasma /ion sputter clean	Not attempted. *Analyzed by NPL using Brongersma	No desiccator, 2 hours, not all solution deposited.

J Phys Chem C Nanomater Interfaces. Author manuscript; available in PMC 2017 October 27.